The determination of molecular orientation in oriented polypropylene by wide angle X-ray diffraction, polarized fluorescence and refractive index measurements

A. P. Unwin, D. I. Bower and I. M. Ward
Department of Physics, University of Leeds, Leeds LS2 9JT, UK
(Received 18 April 1985)

Orientation studies have been undertaken in uniaxially oriented drawn tapes of isotactic polypropylene, using the techniques of wide angle X-ray diffraction, polarized fluorescence and optical birefringence. The results have been interpreted on the basis of a simple two-phase model for orientation of the crystalline and non-crystalline regions. The rise in the orientation of the crystalline regions with increasing draw ratio is extremely rapid, even compared with the pseudo-affine deformation scheme. This result, taken in conjunction with the discontinuous change in the long period, supports the view that the plastic deformation involves a complete breakdown of the original lamellar structure and subsequent recrystallization of the highly oriented drawn material. Further support for this conclusion is obtained from the observation that the orientation of the long fluorescent probes, which might be expected to be constrained to the more highly oriented material, is similar to that measured for the crystalline material by X-ray diffraction.

(Keywords: polypropylene; molecular orientation; polarized fluorescence; X-ray diffraction; birefringence; drawing)

INTRODUCTION

The characterization of molecular orientation in polymers is of interest in at least two major respects. First, there is the question of how molecular orientation in the crystalline and non-crystalline regions develops with increasing plastic deformation. This is often considered in terms of the applicability of theoretical models such as the rubber network model or the pseudo-affine deformation scheme. Secondly, there is the relationship of molecular orientation to physical properties such as modulus or thermal expansion.

In the present paper three methods of characterizing orientation in polymers have been applied to a series of drawn tapes of isotactic polypropylene (iPP). The three methods are wide angle X-ray diffraction, refractive index measurements and the measurement of the intensity of the polarized fluorescence of probe molecules introduced into the bulk polymer in the molten state prior to drawing. The polarized fluorescence technique is of particular interest because it appears to offer a possible means of determining the orientation of the non-crystalline regions, as it seems most unlikely that the comparatively large fluorescent molecules could be present in the crystalline regions. In this paper we compare three similar measures of orientation, the first related to the overall molecular orientation and determined from the refractive index measurements, the second related to the crystalline orientation and determined from the X-ray diffraction measurements and the third related to the orientation of the fluorescent probe molecules. By making the common assumption of a two phase crystalline–amorphous structure, a measure of the non-crystalline orientation has also been obtained by combining refractive index and X-ray diffraction data.

The present studies relate to previous extensive investigations of molecular orientation in iPP by Samuels[1], and a recent investigation using polarized fluorescence by Pinaud *et al.*[2], which was contemporaneous with the research reported here. Nishijima *et al.*[3] have also reported a brief qualitative application of polarized fluorescence to iPP using uranine as the probe molecule. In the present investigation we have followed previous studies in PET[4–6], incorporating as the probe 4,4′-(dibenzoxazolyl)stilbene, which was shown to provide a measure of the orientation of the non-crystalline regions. In their study of iPP Pinaud *et al.* used 1,8-diphenyloctatetraene as the probe and assumed that the fluorescence orientation related to the non-crystalline regions. In this investigation the interpretation of the fluorescence orientation will be regarded as an open question, to be compared with the other experimental measures of molecular orientation and the predictions of theoretical deformation schemes.

DEFINITIONS

When investigating orientation it is convenient to consider an orthogonal set of axes $OX_1X_2X_3$ fixed in the macroscopic sample. For the tapes discussed here OX_3 is fixed parallel to the draw direction whilst OX_1 is constrained to lie in the plane of the tape and OX_2 perpendicular to it.

For transversely isotropic samples we use $\langle P_l(\theta)\rangle$ to denote the average value of the lth order Legendre polynomial, $P_l(\cos\theta)$, where θ is the angle between the axis of the unit under examination and the draw direction. It is convenient to use the subscripts opt, c and p to differentiate between the moment averages obtained from

0032-3861/85/111605-06$03.00

the three techniques employed here, namely, optical dichroism, X-ray diffraction and polarized fluorescence. For example, $\langle P_2(\theta_{opt})\rangle$ is the second moment average obtained from the optical dichroism and $\langle P_4(\theta_p)\rangle$ is the fourth moment average obtained using the polarized fluorescence technique.

EXPERIMENTAL

Preparation of samples

The polymer analysed in this work was isotactic polypropylene (HF-18, Imperial Chemical Industries Limited). Undrawn tapes and film of the polymer were prepared at I.C.I. Plastics Division, Welwyn Garden City, from pellets of the polymer containing a small fraction of the fluorescent compound 4,4'-(dibenzoxazolyl)stilbene. This compound is also known as 2,2'-(vinylene di-*p*-phenylene)-bis-benzoxazole, VPBO, and has the structure shown in *Figure 1*. The molten polymer plus additive was extruded at a temperature of 260°C through a slit die and cast onto a rotating chromed drum with internal water cooling. From there the film, pulled by nip rollers, passed over a series of rollers to the wind up drum, its thickness being monitored during the process.

Subsequently, drawn tapes were produced in two ways. A series of samples with draw ratios in the range 1–7.1 was produced by a continuous drawing method. The tapes ($M_w \sim 450\,000$) were drawn between two rollers, running at different speeds, on a draw frame. The tapes passed over a heated 'pin' immersed in glycerol at a temperature of 110°C, to localize the draw point. The nominal draw ratios of the tapes were calculated from the ratios of the diameters of the feed and wind up rolls and the actual draw ratios were measured from the cross sectional areas of the drawn and undrawn tapes. The cross sectional areas were calculated from the density and weight per unit length of the samples. The measured draw ratio, constant to within 2% along the length of the samples, was found to be ~4% less than the nominal value. Samples with draw ratios in the range 8–13 were produced by drawing film ($M_w \sim 330\,000$) in an Instron tensile testing machine at an air temperature of 110°C, using a draw rate of 5 cm min^{-1}. It should be noted that for these samples, extension occurred in two stages. Initially the sample necked, with a natural draw ratio of approximately 5, and this was followed by a more homogeneous extension. Above a draw ratio of 13, further extension resulted in considerable stress whitening of the specimen and such samples were rejected.

Density

Densities were measured at a temperature of 23°C in a conventional density column, using the liquids diethylene glycol (digol) and propan-2-ol. The column could measure densities in the range 0.88–0.94 g cm^{-3}. When placed in the column, the samples were found to reach their equilibrium positions after 3 h and to be stable there for a time greater than 100 h. Consequently, solvent induced crystallization is negligible during this later period of time. It is difficult to check for solvent induced crystallization in the first 3 h, but the density measured after an immersion time of 1 h revealed a value within 0.002 g cm^{-3} of the final value, and this difference is regarded as insignificant. For convenience, therefore, the sample densities were recorded after an immersion period of 24 h.

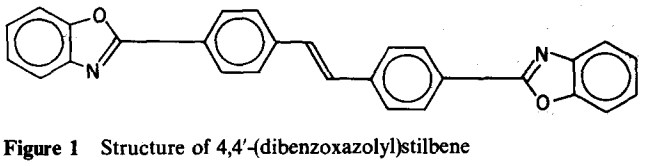

Figure 1 Structure of 4,4'-(dibenzoxazolyl)stilbene

Birefringence

The refractive indices, n_1 and n_3 (electric vector parallel to OX_1 and OX_3 respectively) were measured using an Interphako image splitting interference microscope. The method essentially measures the optical path difference between the sample and an identical thickness of one of a series of liquids, each of known refractive index. This difference is manifested by a fringe shift, and the refractive index of the sample is identified as that of the liquid which produces zero fringe shift. A range of Cargille standard refractive index liquids with index spacings of 0.004 at 25°C was used to provide the relative optical path difference. The transversely isotropic nature of the tapes was checked by measuring all three principal refractive indices of some samples on an Abbe refractometer (Bellingham and Stanley degree scale model).

X-ray diffraction

The usual transmission WAXS technique was used to examine the orientation of the crystallites, the angle between the detector beam and the straight through beam being 2θ. In keeping with convention we identify a 2θ scan as one in which the sample rotates at half the rate of the detector, but a rotation in which only the sample moves we call an ω scan since we define ω to be the angle between the draw direction and a convenient direction in the plane of the rotation. Moreover, the angle between a particular plane normal and the draw direction is denoted by χ. The WAXS technique enables values for $\langle P_2(\chi)\rangle$ and $\langle P_4(\chi)\rangle$ to be found and these can be converted to $\langle P_2(\theta_c)\rangle$ and $\langle P_4(\theta_c)\rangle$ using the equation

$$\langle P_l(\chi)\rangle = \langle P_l(\theta_c)\rangle \langle P_l(\delta)\rangle \quad (1)$$

if the sample is transversely isotropic, and there is no preferred orientation about the *c*-axis. Here θ_c is the angle between the draw direction and the *c* axis in the unit cell and δ is the angle between the *c* axis and the normal to the plane being considered.

The samples were stacks of either 12 or 18 parallel layers of polypropylene tape (dimensions approximately 40 mm, 1 mm and 0.5 mm), and were mounted on the stage of a Siemens diffractometer (type M386-X-A8). A poly(vinyl alcohol) adhesive was used to prepare the stacks, since it provided a strong bond, yet gave little background scatter and no discrete X-ray diffraction peaks. Collimating slits were used to restrict the beam, the widths being selected to reduce machine broadening to a negligible level (< 1°), whilst still leaving measurable intensities.

For each ω scan (i.e. rotation of sample only) the value of 2θ was fixed so that the detector sat at the peak ($2\theta_{pk}$) of the diffraction profile for the relevant reflection. The axis about which the ω scan took place and the consequent corrections to the measured intensities depended on the reflection being examined. Detailed discussion, therefore, will be subdivided accordingly.

The ($\bar{1}13$) reflection

For measurements on the ($\bar{1}13$) reflection, the sample was mounted so that the OX_1X_3 plane was vertical and rotation during an ω scan was about the OX_1 axis, ω being zero when the OX_1X_3 plane was normal to the incident beam (*Figure 2*). Corrections for absorption and the variation in sample volume illuminated by the beam were made (see ref. 7).

The more complicated estimation of the non-crystalline contribution was rendered considerably easier because the work was confined to highly drawn samples, in which the crystalline contribution had decreased to zero at large values of χ and so the background contribution could be read directly. (Only highly drawn samples could be examined because the sample holder blocked the beam at certain values of χ.) The major problem with this method was the possibility that the non-crystalline contribution varied with χ, but this was checked either side of the diffraction peak (i.e. at two values of 2θ either side of the ($\bar{1}13$) reflection) and any variations were found to be insignificant. It was therefore assumed that the background under the diffraction peak itself was constant for changes in χ.

The equatorial reflections

Figure 3 illustrates the arrangement used when examining the equatorial reflections, (040), (110) and (130). In each case the sample was mounted so that the OX_1X_3 plane was normal to the incident beam and the sample was rotated about its OX_2 axis (i.e. the incident beam), ω being measured from OV. The beam was limited by a pin hole placed just before the sample, great care being taken to ensure that the X-ray beam always remained centrally positioned in the sample. With reference to *Figure 3* the draw direction, OX_3, rotated in the vertical plane PVOV' and ω and χ are related by the expression

$$\cos\chi = \cos\theta\cos\omega \qquad (2)$$

and this correction was suitably applied. The only other correction involved the removal of the non-crystalline contribution. Several methods were used to estimate this correction. All corrections were based on the common assumption that the non-crystalline contribution varied much more rapidly with 2θ than with χ and that the latter variation could be neglected, as found for the ($\bar{1}13$) reflection. The different corrections were made as follows.

(a) It was assumed that the ratio, R, of the intensities due to the non-crystalline material at $\chi=0$ for values of $2\theta=2\theta_{pk}$ corresponding to the peak for a particular reflection, and $2\theta=20°$, where there was no crystalline reflection, was constant for all samples. The value of R will change if the non-crystalline material is oriented, but this orientation is later shown to be low compared with the crystalline orientation, and the correction is itself fairly small. R was determined from measurements on a highly oriented sample, where there was no crystalline contribution at $\chi=0°$ for $2\theta_{pk}$ and this enabled the non-crystalline contribution at $2\theta_{pk}$ to be determined from measurements at $\chi=0$, $2\theta=20°$.

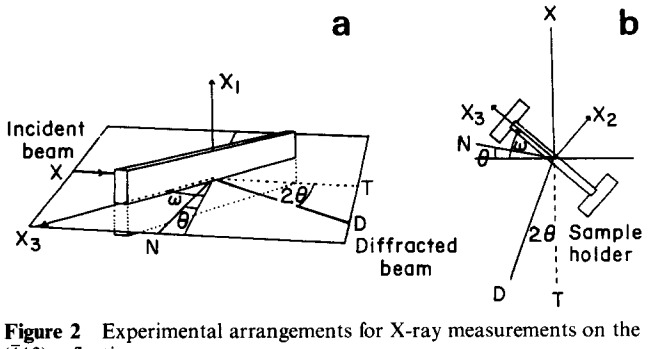

Figure 2 Experimental arrangements for X-ray measurements on the ($\bar{1}13$) reflection

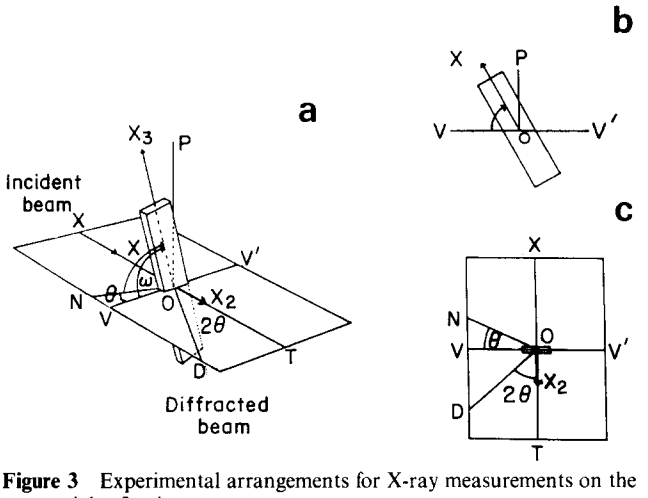

Figure 3 Experimental arrangements for X-ray measurements on the equatorial reflections

(b) It was assumed that the non-crystalline intensity was a linear function of 2θ. Three ω scans were made for values of $2\theta=2\theta_{pk}$ and $2\theta_{pk}\pm1°$. A computer program was then used to remove a trial linear background from the scan, the slope and height of which were allowed to vary until the values of $\langle\cos^2\chi\rangle$ obtained from each of the three ω scans were the same. This was taken to indicate that the correct background had been found. This correction assumes that the shape of the 2θ plot is independent of χ (but not, of course, the absolute intensity).

(c) It has been shown[8] that the expression for the most probable distribution

$$N_{mp}(\theta)=\exp\left(\sum_l \alpha_l P_l(\cos\theta)\right) \qquad (3)$$

where $l=0$, 2 and 4, is often a good approximation to the true distribution function if α_0, α_2 and α_4 are chosen so that the distribution has the correct values of $\langle P_0(\cos\theta)\rangle$, $\langle P_2(\cos\theta)\rangle$ and $\langle P_4(\cos\theta)\rangle$.

A least squares fit of the experimental data to a curve of the form given in equation (3), allowing also for a constant background, was performed. The program returned values of α_0, α_2, α_4 and the background. These values were then used to predict the form of the curve for $\chi<\theta$ (see *Figure 4*) and to obtain values for $\langle P_2(\theta_c)\rangle$ and $\langle P_4(\theta_c)\rangle$. It was not possible to measure the diffracted intensity for $\chi<\theta$ and $\chi>\pi-\theta$ because of the experimental arrangement.

SAXS

Small angle X-ray scattering patterns were obtained using a Searle X-ray camera, with a sample to photographic film distance of 20 cm.

Polarized fluorescence

The measurement of the orientation of the fluorescent probes was performed using basically the same technique and apparatus as Nobbs *et al.*[4]. The apparatus, a slight

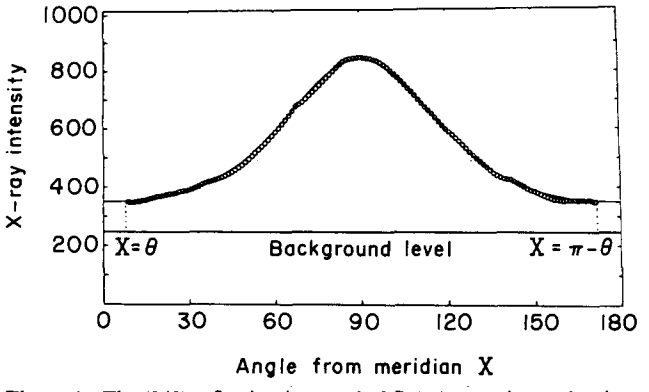

Figure 4 The (040) reflection in sample 3C. (○): experimental points; (—): equation (3)

modification of that used by Nobbs *et al.* is shown in *Figure 5*. Light of wavelength 365 nm from the mercury arc lamp is selected by the first monochromator before being allowed to hit a beam splitter which directs a fraction of the light to the monitor. The straight through light is allowed to fall in a parallel beam onto the sample. The second monochromator allows fluorescent light of wavelength 469 nm emitted from the sample to pass to the detector. For each oriented sample the intensities recorded were those for parallel and crossed polarizers with the sample draw direction (OX_3) alternately parallel and perpendicular to the direction of polarization of the exciting light.

The samples were mounted in a liquid of similar refractive index on a microscope slide and located using a rectangular cover slip. The liquid used was a Cargille standardized liquid of refractive index 1.5046 at 25°C for light of wavelength 486 nm. (Note that the liquid did not produce any fluorescent light at the observing wavelength.) The liquid was used in order to minimize both reflection at the sample boundaries and the depolarizing effects due to the irregularity of the sample surfaces.

Corrections for absorption and stray light were applied to the measured intensities. For measurements on the random sample it was also necessary to apply a correction for the depolarizing effects due to spherulites as suggested by Pinaud *et al.*[2]. For the analysis of the results it was necessary to make certain assumptions about the nature of the probe. In the model used here the difference between the azimuthal angles for the absorption and emission axes was assumed to be random. The corrected intensities and the parameter determined from the random sample, together with initial values for the mean polar angles of the absorption and emission axes were fed into a program which used an iterative procedure to calculate the values of $\langle P_2(\theta_p)\rangle$ and $\langle P_4(\theta_p)\rangle$, consistent with the assumptions embodied in the model described above. This model corresponds to model 1 described by Nobbs *et al.*[4]. They also described a second model but this was rejected here because it gave mathematically impossible values for $\langle P_4(\theta_p)\rangle$. The second model was also rejected by Nobbs *et al.* on somewhat different grounds.

RESULTS

Table 1 shows that samples with draw ratios less than 8 had a density of 0.902 ± 0.001 g cm^{-3}, which corresponds to a crystallinity of 59.4% assuming the densities of the crystalline and non-crystalline phases to be 0.938 and 0.854 g cm^{-3} respectively[9]. The results for the refractive indices n_1 and n_3 for a wavelength of 589.6 nm and a temperature of 25°C are also presented in *Table 1*, as are the corresponding birefringences. The refractive indices are accurate to 0.001, and the birefringences to 0.0005. *Table 2* shows the refractive index measurements obtained from the Abbe refractometer. There is one essential difference between the physical interpretations of the results obtained from the two methods used here. The Interphako measures the mean refractive index through the sample thickness, whereas the Abbe refractometer measures the refractive index in the surface layer. Since the values obtained from these two methods are in good agreement there is little reason to suspect the existence of large differences in the properties of the tapes between the surfaces and the inner material. Moreover, the agreement between n_1 and n_2 in *Table 2* shows that the samples are transversely isotropic.

Figure 6 shows the variation of $\langle P_2(\theta_{opt})\rangle$, evaluated assuming a value of 0.038 for Δn_{max}, with draw ratio. This value for Δn_{max} agrees well with measurements on highly drawn samples. Also shown is the predicted variation according to the pseudo-affine deformation scheme, which considers the rotation of stiff rods in a softer matrix, together with the variations in $\langle P_2(\theta_c)\rangle$ and $\langle P_2(\theta_p)\rangle$.

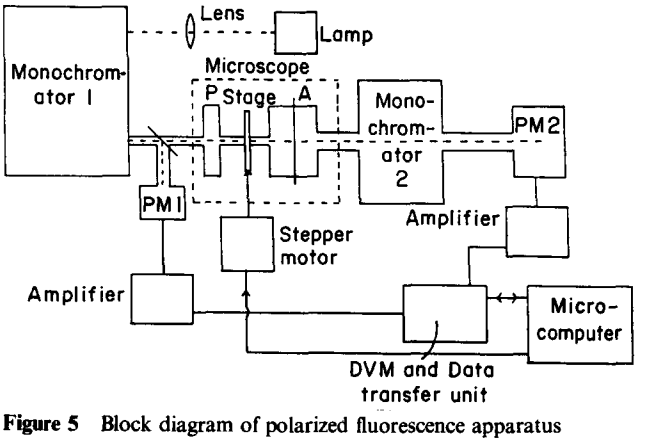

Figure 5 Block diagram of polarized fluorescence apparatus

Table 1 Characterization of polypropylene samples. Series 3 samples produced by continuous drawing. Series 4 samples produced on Instron

Sample	Draw ratio		Density	Interphako results		
	Nom[a]	Meas[b]	(g cm^{-3})	n_1	n_3	Δn
3	1.00	1.0	–	–	–	–
3A	1.28	1.22	0.9010	–	–	–
3B	1.34	1.30	0.9010	1.497	1.504	0.0068
3C	1.5	1.38	0.9010	1.496	1.505	0.0087
3D	1.68	1.52	–	–	–	–
3E	2.0	1.92	0.9028	1.494	1.509	0.0147
3F	2.06	1.84	–	–	–	–
3G	2.56	2.38	–	1.493	1.512	0.0192
3H	3.00	2.86	0.9024	1.492	1.514	0.0218
3I	3.75	3.5	0.9015	1.490	1.516	0.0260
3J	5.0	4.8	0.9010	1.489	1.517	0.0282
3K	7.3	7.1	0.9010	1.487	1.520	0.0327
4L	–	9.3	0.9042	1.4885	1.522	0.0335
4M	–	9.8	0.9040	–	–	–
4N	–	11.7	0.9040	1.490	1.525	0.0354
4O	–	12.6	–	–	–	–

[a] Nom – nominal values obtained from speeds of windup and feed rollers
[b] Meas – values obtained from measurements of changes in cross-sectional areas

Table 2 Refractive indices as determined by Abbe refractometer

Sample	Draw ratio	n_1	n_2	n_3	Δn
3B	1.32	1.496	1.496	1.503	0.007
3C	1.38	1.495	1.496	1.505	0.010
3E	1.92	1.491	1.491	1.509	0.017
3I	3.5	1.488	1.488	1.514	0.026
3J	4.8	1.486	1.487	1.516	0.030
4L	9.3	1.489	1.489	1.523	0.034

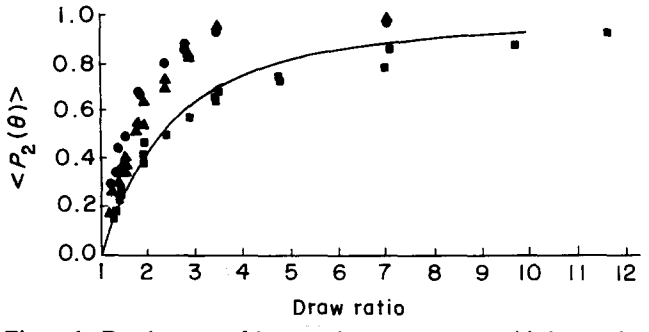

Figure 6 Development of the second moment average with draw ratio. (■): $\langle P_2(\theta_{opt})\rangle$; (●): $\langle P_2(\theta_c)\rangle$; (▲): $\langle P_2(\theta_p)\rangle$

The values for $\langle P_2(\theta_c)\rangle$ and $\langle P_4(\theta_c)\rangle$ for samples of draw ratio less than 2.5 are shown in *Table 3*. The letters (a), (b) and (c) refer to the different methods, discussed above, used to determine the non-crystalline background. Generally there is good agreement between the values obtained from each of the different methods used to evaluate the background. This is not particularly significant for methods (a) and (b), but the general agreement with method (c) does suggest that the experimental distribution can be represented well by equation (3). This is illustrated more clearly in *Figure 4*, where both the experimental data and the theoretical curve (equation (3)) are shown.

For samples with draw ratios >2.5, $\langle P_l(\theta_c)\rangle$ could be determined from any one of four reflections. Values of $\langle P_2(\theta_c)\rangle$ and $\langle P_4(\theta_c)\rangle$ were obtained from all four reflections for only one sample, although they were calculated from more than one reflection for several other samples. *Table 4* illustrates these comparisons. Again there is good agreement between the results and there is no obvious merit in taking one set of results in preference to another. For comparative purposes, however, attention will be focused, where possible, on the results of measurements on the (040) reflection since these provide the most complete set. These results are gathered in *Table 5*. The results quoted in *Table 5* for samples of low draw ratio are those calculated using method (b) to evaluate the background. This method has been chosen in preference to method (a) because the ratio R, used in the latter approach, might vary from sample to sample for the reason mentioned earlier. The disadvantage of method (c) is the use of the additional assumption that the distribution is the most probable one.

The value of the long period for the isotropic sample was found to be 105 Å, whilst that for drawn samples with $\lambda < 7$ was 150 Å. Samples with draw ratios greater than 7 did not give a detectable two point pattern.

The results obtained for $\langle P_2(\theta_p)\rangle$ and $\langle P_4(\theta_p)\rangle$ (an average of two or three different measurements in each case) are given in *Table 6*. *Figure 7* gives the dependence of $\langle P_2(\theta)\rangle$ on $\langle P_4(\theta)\rangle$ for the X-ray and polarized fluorescence results, and that which would be expected for a pseudo-affine deformation scheme. Finally, *Figure 8* shows the variation with draw ratio of the amorphous orientation average, $\langle P_2(\theta_a)\rangle$, calculated assuming a two phase model approach and using some of the different intrinsic birefringences[10,11], commonly quoted for iPP. The form birefringence has been ignored, but the contribution to the total birefringence that this might have has been discussed by Normandin and Legrand[12], and although, under certain circumstances, this may be significant ($\sim 10\%$) it is found to have an insignificant effect on the shapes and relative trends of the curves for $\langle P_2(\theta_a)\rangle$ shown in *Figure 8*.

DISCUSSION

It can be seen from *Figure 6* that the X-ray diffraction results show that the orientation of the chain axes in the crystalline regions increases very rapidly with draw ratio

Table 3 Comparison of $\langle P_2(\theta_c)\rangle$ and $\langle P_4(\theta_c)\rangle$ for iPP samples using different methods to determine the non-crystalline background

	(a)		(b)		(c)	
Sample	$P_2(\theta_c)$	$P_4(\theta_c)$	$P_2(\theta_c)$	$P_4(\theta_c)$	$P_2(\theta_c)$	$P_4(\theta_c)$
3A	0.284	0.053	0.289	0.054	0.359	0.068
3B	0.323	0.075	0.338	0.078	0.339	0.088
3C	0.431	0.124	0.446	0.129	0.411	0.119
3D	0.442	0.155	0.491	0.173	0.505	0.184
3E	0.672	0.310	0.675	0.312	0.682	0.315
3F	0.668	0.329	0.682	0.336	0.653	0.327

Table 4 Comparison of $\langle P_2(\theta_c)\rangle$ and $\langle P_4(\theta_c)\rangle$ evaluated from different reflections for iPP samples of draw ratio >2.5

		Reflection			
Sample		(110)	(040)	(130)	($\bar{1}$13)
3I (3.50)	$P_2(\theta_c)$	0.928	0.935	0.942	0.954
	$P_4(\theta_c)$	0.780	0.802	0.820	0.853
3H (2.86)	$P_2(\theta_c)$		0.880		0.883
	$P_4(\theta_c)$		0.657		0.661
3H (2.86)	$P_2(\theta_c)$		0.856	0.860	
	$P_4(\theta_c)$		0.625	0.618	

Table 5 Results of $\langle P_2(\theta_c)\rangle$ and $\langle P_4(\theta_c)\rangle$ for drawn polypropylene

Sample	$P_2(\theta_c)$	$P_4(\theta_c)$	Sample	$P_2(\theta_c)$	$P_4(\theta_c)$
3A	0.289	0.054	3F	0.682	0.336
3B	0.338	0.078	3G	0.800	0.507
3C	0.446	0.129	3H	0.868	0.641
3D	0.491	0.173	3I	0.935	0.802
3E	0.675	0.312	3K	0.968	0.899

Table 6 Values of $\langle P_2(\theta_p)\rangle$ and $\langle P_4(\theta_p)\rangle$ for samples of differing draw ratios. $\langle P_l(\theta_p)\rangle = \langle P_l(\cos\theta_p)\rangle$

Sample	$P_2(\theta_p)$	$P_3(\theta_p)$	Sample	$P_2(\theta_p)$	$P_4(\theta_p)$
3A	0.227	0.026	3F	0.534	0.223
3B	0.297	0.055	3G	0.714	0.470
3C	0.307	0.045	3H	0.840	0.686
3D	0.374	0.086	3I	0.962	0.920
3E	0.568	0.252	3K	0.999	1.00

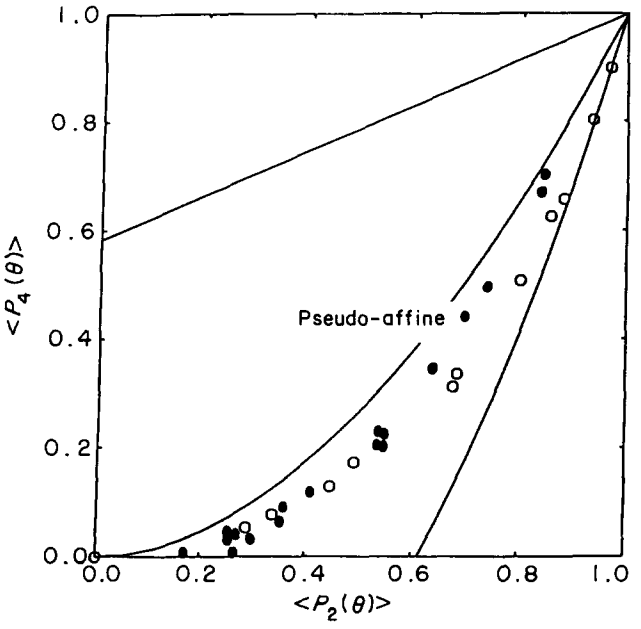

Figure 7 $\langle P_2(\theta)\rangle$–$\langle P_4(\theta)\rangle$ plot of X-ray and polarized fluorescence results. (○): X-ray; (●): polarized fluorescence

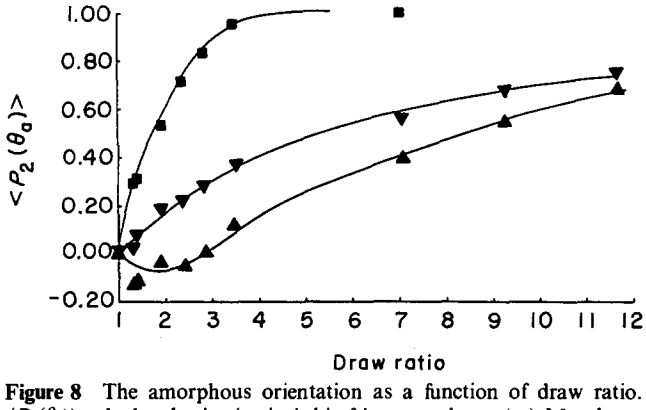

Figure 8 The amorphous orientation as a function of draw ratio. $\langle P_2(\theta_a)\rangle$ calculated using intrinsic birefringences due to (▲): Masuko *et al.*; (▼): Samuels. (■): $\langle P_2(\theta_p)\rangle$

to maximum orientation, at a much greater rate than the pseudo-affine deformation scheme predicts. The latter scheme follows the proposal of Kratky[13] that the crystallites orient like rigid rods embedded in a matrix of deformable material. This approach is clearly incorrect, and the results are consistent with the proposals of Peterlin[14] which involve the breakdown of the initial lamellar structure and recrystallization so that new blocks are formed where the crystalline regions are very highly oriented and there is a characteristic long period determined by the draw temperature, which reflects a regular structure of alternating crystalline and non-crystalline regions.

The refractive index measurements give an optical orientation average which increases comparatively slowly with increasing draw ratio, at a rate which is quite close to that predicted by the pseudo-affine deformation scheme. This result has been noted previously[15] as has the close coincidence of the measured $\langle P_2(\theta)\rangle/\langle P_4(\theta)\rangle$ ratio with that predicted by the pseudo-affine deformation scheme[2] and which is shown for the probes and crystalline regions in *Figure 7*. Taken together with the X-ray measure of crystalline orientation, the birefringence results suggest that the orientation of the non-crystalline component remains comparatively low and is not simply related to that of the fluorescent molecules. This expectation is confirmed by the quantitative attempts to calculate the non-crystalline orientation shown in *Figure 8*, irrespective of the detailed assumptions.

Finally it is to be noted that the orientation functions obtained from polarized fluorescence are very similar in their development with draw ratio to that for the crystalline orientation, and this is true for both $\langle P_2(\theta)\rangle$ and $\langle P_4(\theta)\rangle$. This result suggests that the fluorescent probes fit into the more aligned regions during the drawing process, prior to the recrystallization which occurs. It is similar to the results obtained in PET[6], where the fluorescence orientation averages were very similar to the infra-red orientation averages observed for the *trans* conformations, from which it was concluded that the probes fitted into the non-crystalline *trans* sequences. This similarity between results for iPP and PET is probably due to the large length of the probes compared with individual molecular segment lengths, so that they can only fit into long sequences of aligned material. The fluorescence orientation averages would then be similar to the crystalline orientation averages, with the fluorescent probes probably lying on the surface of crystallites. It is interesting to recall that when fluorescent probes were first incorporated in polymers by Morey[16] he concluded that their orientation reflected that of the crystalline regions.

CONCLUSIONS

The techniques of optical dichroism, polarized fluorescence and X-ray diffraction have been combined to examine oriented polypropylene tapes. The wide and small angle scattering results support the view that orientation in polypropylene is accompanied by lamellar breakdown and subsequent recrystallization. The good correlation between the X-ray and polarized fluorescence measurements is attributed to the positioning of the fluorescent probes in the more highly aligned regions during drawing and prior to recrystallization.

REFERENCES

1 Samuels, R. J. *J. Polym. Sci. A-2* 1968, **6**, 2021
2 Pinaud, F., Jarry, J. P., Sergot, Ph. and Monnerie, L. *Polymer* 1982, **23**, 1575
3 Nishijima, Y., Fujimoto, T. and Onogi, Y. *Rep. Prog. Polym. Phys. Jpn* 1966, **9**, 457
4 Nobbs, J. H., Bower, D. I., Ward, I. M. and Patterson, D. *Polymer* 1974, **15**, 287
5 Nobbs, J. H., Bower, D. I. and Ward, I. M. *Polymer* 1976, **17**, 25
6 Nobbs, J. H., Bower, D. I. and Ward, I. M. *J. Polym. Sci., Polym. Phys. Edn.* 1979, **17**, 259
7 Decker, B. F., Asp, E. T. and Harker, D. *J. Appl. Phys.* 1948, **19**, 388
8 Bower, D. I. *J. Polym. Sci., Polym. Phys. Edn.* 1981, **19**, 93
9 Alexander, L. E. 'X-ray Diffraction Methods in Polymer Science', Wiley-Interscience, New York, 1969, p. 480
10 Samuels, R. J. *J. Polym. Sci. A-2* 1968, **6**, 1101
11 Masuko, T., Tanaka, H. and Okajima, S. *J. Polym. Sci. A-2* 1970, **8**, 1565
12 Normandin, L. M. and Legrand, D. G. *J. Polym. Sci. A-2* 1969, **7**, 231
13 Kratky, O. *Kolloid Z. Z. Polym.* 1933, **64**, 213
14 Peterlin, A. and Balta-Calleja, F. J. *J. Appl. Phys.* 1969, **40**, 4238
15 Pinnock, P. R. and Ward, I. M. *Brit. J. Appl. Phys.* 1966, **17**, 575
16 Morey, D. R. *Textile Research* 1933, **3**, 325